Evolution of an Electron Current Layer Prior to Reconnection Onset

Nagendra Singh

Phys. Rev. Lett. **109**, 145001 — Published 1 October 2012

DOI: 10.1103/PhysRevLett.109.145001

Evolution of an Electron Current Layer Prior to Reconnection Onset

Nagendra Singh

Department of Electrical and Computer Engineering, University of Alabama, Huntsville, AL 35899, USA.

Huntsville, Alabama, 35899, USA.

Abstract. Electron current layers (ECLs) are the sites where magnetic reconnection (MR) initiates in a current sheet (CS). Using three-dimensional particle-in-cell (3DPIC) simulations, we study the plasma processes that occur in an ECL as it evolves rapidly over a short time scale much shorter than the ion cyclotron period. The processes include its thinning, generation of electrostatic instabilities, trapping and heating of electrons in growing waves, its re-broadening, generation of anomalous resistivity and eventually the generation of large-amplitude magnetic fluctuations. These fluctuations could be interpreted in terms of electron tearing and/or Weibel instabilities, which are commonly invoked as mechanisms for the MR onset. The widths of the broadened ECL are compared with those measured in the MRX experiment, showing excellent agreement.

1. Introduction

Mechanism for the onset of magnetic reconnection is a long standing unsolved problem in plasma physics. Several studies [1-4] have shown that the fast magnetic reconnection initiates in electron current layers (ECLs). But the sequence of plasma processes leading to reconnection remains unresolved. The half width (w) of an ECL is a critically important parameter as it determines the current density and the plasma instabilities which ensue. Measurements in MRX experiments [5, 6] revealed that the half widths of electron current layers (ECLs) are w ~ 5-8 λ_e,

where λ_e is the electron skin-depth; such widths are much larger than w ~ 1-2 λ_e found in two-dimensional (2D) simulations [6-8]. Refs. [5] and [6] suggest that the three-dimensional (3D) effects in the experiments are responsible for the creation of the wider ECLs. Prior 3D simulations [9-10] showed that even in 3D first a thin ECL forms with w ~ 2 λ_e and eventually the ECL broadens owing to increased kinetic pressure in the ECL as the current-driven electrostatic instabilities (CDEIs) in the thinnest ECL (w ~2 λ_e) heat the plasma. We report here that the plasma processes, which rapidly occur in an ECL at electron time scale, not only cause its re-broadening, but also generate the conditions that are commonly invoked for the onset of magnetic reconnection. The CDEIs generate electron temperature anisotropy by initially heating the electrons in the direction of current [9]; this could trigger Weibel instability (WI) [11]. The trapping of the electrons by the waves generates anomalous resistivity (η_a), which enhances the growth of the electron tearing instability (ETI) [12]. For the electron heating along the current, the ETI and WI could couple, generating the magnetic field perturbations essential for reconnection onset [13]. For the first time we discuss here the sequential occurrences of the plasma processes during the pre-onset evolution of an ECL. We also compare the half widths of the ECL found in the 3D simulations with laboratory measurements [3, 5, 6], showing good agreement.

2. Method of Simulation

We utilized a fully 3-D electromagnetic PIC code with relativistic effects included [9, 10]. We simulate a three-dimensional (3-D) volume, $L_x \times L_y \times L_z$, with anti-parallel magnetic fields:

$$\mathbf{B}\,(z) = B_o \tanh[(z-z_c)/L]\ \mathbf{a_x}, \qquad (1)$$

where B_o is the magnetic field at distances far away from the central plane $z = z_c = L_z / 2$, $\mathbf{a_x}$ is a unit vector along the x axis, L is the half width of **B**(z). This field is applied to uniform plasma

without an initial current. B_o is adiabatically increased from zero to its final value over about 10 electron cyclotron period. The current sheet develops in response to the applied magnetic stress as in laboratory experiments [2, 3].

The initial plasma has uniform density n_o and Maxwellian electrons and ions having temperatures $T_e = T_o$ and $T_i = 2T_o$, respectively. We incorporated periodic boundary conditions along x and y on both particles and fields. Along z we used conducting boundary conditions for the fields while the particle boundary conditions were varied in different simulations. In the simulations described here, the particles leaving the simulation box at boundaries z = 0 and L_z are not re-circulated, instead they are replaced by new ones from the Maxwellian distributions having the same temperatures as the initial plasma loaded in the simulation box. The fields and particles are updated using a time step $\Delta t = 0.02\omega_{po}^{-1}$ and spatial grid size $\lambda_{do} = V_{teo}/\omega_{po}$, where ω_{po} is the electron plasma frequency, V_{teo} is the electron thermal velocity in the initial plasma. We used ion to electron mass ratio M/m =1836, $\Omega_{eo}/\omega_{po} = 0.5$, $C/V_{teo} = 10$, $L = 36\lambda_{do} = 3.6\lambda_e$ $L_z = 256\lambda_{do} = 25.6\lambda_e$ and $L_x = L_y = 32\lambda_{do}$, where Ω_{eo} is the electron cyclotron frequency with B_o and C is velocity of light. The units used in the following discussion are: distance (λ_{do}), time (ω_{po}^{-1}), velocity (V_{teo}), electric fields ($T_{eo}/e\lambda_{do}$), magnetic fields ($e\omega_{po}/m$) and current ($J_{th} = n_o e V_{teo}$).

3. Electron Current Layer

Figure 1 shows the evolution of the current profile $J_y(z)$ averaged over the x-y plane. Electrons primarily carry the current. In response to the applied **B**(z) in (1), first a broad ECL forms as seen at t =100; subsequently it thins until t ~ 500 and it re-broadens at later times (Fig. 1). Such thinning and re-broadening of an ECL can be seen from the experimental results reported in Ref. [3]. By fitting a Harris type profile like in (1) to the evolved profile of $B_x(z)$ at t = 500, we find that the minimum half width is $w \cong 2\lambda_e$, as seen in 2DPIC simulations [6-8].

When the ECL attains the width w ~ $2\lambda_e$, the total pressure, consisting of magnetic and kinetic pressures, becomes nearly constant across it [9]. Such thinning is essential for plasma instabilities, which precondition the ECL for the onset of fast reconnection [14]. The thinning is caused by plasma flows from the outer regions of the ECL to its central region near z ~ $L_z/2$ = $128\lambda_{do}$. The flow develops due to the **J**×**B** force on the current-carrying magnetized electrons. But the ECL does not remain this thin for long; it tends to re-broaden with the maximum current slowly reducing until t ~800 and eventually the current in the central CS severely disrupts, leaving a bifurcated ECL. In couple of ion plasma periods (~ 500), the ECL becomes quite broad (Fig. 1).

Table 1 shows the ECL width for t ≥ 500; w ranges from $1.8\lambda_e$ to $6\lambda_e$ as found from 2D simulations [8] and the MRX experiment [5, 6]. The broadening and eventual current disruption in the central region near z~128 for t ≥ 900 (Fig. 1) result from trapping of electrons by plasma waves driven by the current in the thin ECL, as discussed in the next two sections.

Table 1. Temporal evolution of the current sheet in response to plasma heating by waves

t (ω_{po}^{-1})	500	600	700	800	900
w (λ_e)	1.8	2.5	3	4.5	6

4. Plasma Waves

Figures 2a-2f show the temporal evolution of wave electric (E_x, E_y and E_z) and magnetic (b_x, b_y, b_z) fields. We notice that the fluctuations in the magnetic fields b_y and b_z are minimal until t ~ 800. Over the same time period the perturbations in the x-component of the magnetic field, b_x, are associated with the thinning of the ECL (Fig. 1); the perturbation b_x plus **B**(z) in (1) give the

thinned current sheet as seen near t ~ 500 (Fig. 1). In contrast to the behavior of **B**, the fluctuations in the electric field components in Figs. 2a-2c begin to grow as early as t ~ 200. The instability starts out as predominantly electrostatic (ES). Figure 3a-3c shows the wave structures in E_x, E_y, and E_z in the x-z (y=16) (top) and x-y (z=128) (bottom) planes, respectively. The growing oscillations are confined in the central region of the ECL (top panels, Figs. 3a-3c). Fourier analysis of the spatial oscillations show that the dominant modes have $0.5 < k_y\lambda_{do} < 1$ and $k_x\lambda_{do} \sim 1$. Such wave numbers are comparable with the wave numbers expected for the Buneman type instability [15] or oblique ion modes in a plasma with hot ions [16], for which we have $k_y \sim \omega_{pe}/V_{edy}$, where V_{edy} is the average electron drift.

Fig. 4 shows the electron and ion velocity distribution functions at t = 500; drift $V_{edy} = -1.045V_{teo}$, electron temperature $T_{ey} = 2.\ 34T_o$ and ions have the initial $T_i = 2T_o$. Note that the electrons are already heated by a factor of 2.34 and $V_{edy} < V_{et} = 1.5\ V_{teo}$. The temporal evolution of T_{ey} and T_{iy} are shown in Figs. 5a. Note that initially we have $T_{ey}/T_{iy} = 0.5$ and T_{ey} remains smaller than T_{iy} till t ~ 500. Eventually, for $t \geq 500$ the heated electrons have $T_{ey}/T_{iy} > 1$, which creates the favorable condition for the ion modes [15]. Since J_y (Fig. 1) and the drift V_{edy} (Fig. 5b) remain nearly constant over $300 < t < 700$, the increasing ratio T_{ey}/T_{iy} (Fig. 5a) facilitates the wave growth (Figs. 2a-2c) after t ~ 500.

5. Anomalous Resistivity

Figure 5b shows the plots of electron drift as a function of time. We measure the anomalous resistivity by calculating the rate of change in the average electron momentum in the center of the ECL ($112 < z/\lambda_{d0} < 144$); the anomalous collision frequency is $\nu_a(t) = V_{edy}^{-1}dV_{edy}/dt$ (e.g. see Watts et al. [17]). Figure 5c shows the temporal evolution of $\nu_a(t)$, which fluctuates before t ~

500 and afterwards it grows faster and faster until t ~ 850. The maximum anomalous frequency reaches a value as high as $\nu_{max} \sim 0.6\ \omega_{pi}$, where ω_{pi} is the ion plasma frequency. The fast growth in ν_a is accompanied by electron and ion heating (Fig. 5a). As the electron drift decreases (Fig. 5b), ν_a, T_{ey} and T_{iy} grow, and electrons and ions clump strongly due to trapping by the wave. Figure 6 shows the state of the electron clumping at t ~ 800. A similar clumping occurs for the ions. The three-dimensional size of the clumps is a few Debye lengths. The clumps generate spiky electric fields in the central ECL, but not electron holes since electrons are unmagnetized in the central CS.

Dupree [18] developed a theory for anomalous resistivity based on the formation of electron and ion clumps interacting as macro-particles giving an enhanced plasma resistivity,

$$\eta_D = 9 \times 10^8\ (k\ \lambda_d / \omega_{pe}) \quad \Omega\text{-m}, \qquad (2)$$

where k is the wave number. From (2) with $k\lambda_d \sim k_y\lambda_d \sim 1$ we obtain a theoretical value of the resistivity $\eta_D = 10^{-2}\ (\omega_{pe}\varepsilon_o)^{-1}$. From Fig. 6c we have $\nu_{a,\ max} \sim 0.6\omega_{pi}$ at t ~ 850 and the corresponding resistivity is $\eta_a = (\nu_{max}/\omega_{pi})\ (m/M)^{1/2}\ (\omega_{pe}\varepsilon_o)^{-1} = 1.2\times10^{-2}\ (\omega_{pe}\varepsilon_o)^{-1}\ \Omega$-m, which is in excellent agreement with the above theoretical prediction [18]. The resistivity discussed here primarily arises from the wave-article interactions; other terms in the Ohm's law such as $\mathbf{J}\times\mathbf{B}$ and pressure gradients are negligibly small near the mid plane (z =128) of the simulation.

Accompanying the increase in η_a (Fig. 5c), the magnetic field perturbations b_y and b_z develop large-amplitude fast fluctuations after t ~ 800 (Figs. 2e and 2f)). Figures 7a-7c show that the **B** vectors, which remain antiparallel until t ~700, begin to develop b_z component in the central part of the ECL for t ≥ 800. Since the magnetic fluctuations grow with the increase in η_a, we suggest that they are generated by electron tearing instability (ETI) with its growth rate enhanced by η_a [12]. It is also likely that the coupling between WI and ETI generate the

fluctuations [13]. Our simulation is not large enough to yield fully developed reconnection and we stop at t ~1000.

6. Conclusion and Discussion

Using 3D kinetic simulations we found that the processes that occur in an ECL before MR onset include current-driven instabilities, plasma heating, re-broadening of the ECL, generation of electron thermal anisotropy, anomalous resistivity and eventual onset of the tearing in the ECL.

Ren et al. [1] and Ji et al. [2] reported much wider ECLs from the MRX experiments than those seen in 2D simulations and they suggested that the difference could be due to the third dimension in the experiment. Our simulations show that the current in the 'third' out-of-plane direction y drives instabilities, which heat the plasma in the current sheet and thereby the width of the current layer increases (Table 1) due to enhanced plasma pressure. The broadening of the ECL occurs in a time of about $\tau < 500$ or about $\sim 2\omega_{pi}^{-1}$, where ω_{pi}^{-1} is the ion time scale. For the argon ions and plasma density $n \sim 10^{19}$ m^{-3} in the MRX, the widening could be achieved in a few nanoseconds making it difficult to measure the thinnest ECL with $w \sim 2\lambda_e$.

The CDEIs cause current disruption by trapping electrons in its central part. The current disruption in the central CS is the primary cause of the bifurcation of the ECL shown in Fig. 1. The Cluster observations of bifurcated current sheets in the magneto-tail [4] directly deal with thin ECLs like that seen in our simulations [9]. In contrast, the bifurcated CSs reported in Runov et al. [19] are much wider, having $w \sim d_i$, the ion inertial length. The entire evolution of the ECL (Fig. 1), showing its thinning followed by widening and eventual bifurcation, is similar to experimental results reported in Ref. [3].

Commonly invoked plasma processes for MR onset are (i) Generation of anomalous resistivity by plasma instabilities, the role of the resistivity in enhancing the growth rate of the ETI [12], generation of electron temperature anisotropy associated with the heating of the electrons in the direction of the ECL current [11] and the role of the thermal anisotropy in the generation of WI, ETI and their coupling [11, 13]. For the first time we highlight that these processes are integral features of an evolving ECL. These processes follow in a sequence involving thinning of an ECL, generation of electrostatic instabilities, electron and ion trapping by the growing waves generating anomalous resistivity and causing plasma heating, followed by sudden generation of magnetic fluctuations, including the B_z component [9, 10]. This field component is deemed essential for the reconnection onset [11]. Previously we have shown that heating first occurs in the direction of the current [9], a thermal anisotropy which favors both WI [11] and ETI [13]. However, the thermal anisotropy lasts for a short while; electrons are isotropized by the scattering by the developing electromagnetic fluctuations [9]. Can the developing anomalous resistivity facilitate the growth of ETI to large amplitudes [12], seeding the reconnection? We need much larger 3D simulations to demonstrate this. We hope to address this issue in future. We mention that the ECL evolutionary features reported here will be relevant to the high-resolution measurements planned for the NASA's Magnetospheric Multi-Scale (MMS) mission to be launched in 2014.

Acknowledgement: This work was supported by a NSF grant ATM0647157. The computing for this work was performed on the Alabama Supercomputer Center.

References

[1] J. F. Drake, M. A. Shay, and M. Swisdak, Phys. Plasmas 15, 042306 (2008).

[2] H. Ji et al., Phys. Rev. Lett. 92, 115001 (2004)

[3] J. Egedal et al., Phys. Rev. Lett. 98, 015003 (2007).

[4] J. Wygant, et al., J. Geophys. Res., 110, A09206(2005).

[5] Ren et al., Phys. Rev Lett. 101, 085003 (2008)

[6] Ji et al., Geophys. Res. Lett. 35, L13106 (2008)

[7] M. A. Shay, J. F. Drake and M. Swisdak, Phys. Rev. Lett. 99,155002 (2007).

[8] H. Karimabadi, W. Daughton and J. Scudder , Geophys. Res. Lett. 34 L13104 (2007).

[9] N. Singh et al., Nonlinear Proc. Geophys. 13, 509 (2006).

[10] N. Singh et al., J. Geophys. Res. 115, A04203 (2010).

[11] R. A. Treumann, R. Nakamura, and W. Baumjohann, Ann. Geophys., 28, 1935(2010)

[12] M. Lyutikov, arXiv:0705.3186v (2007).

[13] H. Karimabadi, W. Daughton, and K. B. Quest, Geophys. Res. Lett., 31, L18801, 2004.

[14] N. Singh, Phys. Rev. Lett. 107, 245003 (2011)

[15] O. Buneman, Phys. Rev. Lett 115, 503, 1959.

[16] B. D. Fried, and R. W. Gould, Phys. Fluids 4, 139, 1961.

[17] C. E. J. Watt, R.B. Horne, and M.P. Freeman, Geophys. Res.Lett. 29, 1004 (2002).

[18] T. H. Dupree, Phys. Rev. Lett. 25,789, 1970.

[19] A. R. Runov et al., Geophys. Res. Lett., 30(2), 1036, doi:10.1029/2002GL016136.

Figure Captions

Fig. 1. Current $J_y(z, t)$; the numbers in the panels are normalized time; the ECL thins until $t \sim 500\omega_{po}^{-1}$ and then it broadens.

Fig. 2. Temporal evolution of fluctuations in (a) E_x, (b) E_y, (c) E_z and in magnetic fields (d) b_x, (e) b_y and (f) b_z.

Fig. 3. Wave structure at t = 700: $E_x(x,z)$, $E_y(x,z)$ and $E_z(x,z)$ in top panels from left to right in the x-z plane at y = 16 and bottom panels in the x-y plane at z = 128.

Fig. 4. Electron and ion Velocity distribution functions at t= 500

Fig. 5. Temporal evolution: (a) Electron (solid) and ion (dotted) temperatures T_{ey} and T_{iy}, (b) electron drift V_{edy} and (c) anomalous collision frequency ν_a.

Fig. 6. Spatial distribution of electrons in the x-y plane in the central ECL ($124 < z < 132$); bunched electrons are seen. The 3D size of a bunch is a few Debye lengths.

Fig. 7. Vector plot of **B** in the x-z plane at (a) t = 700, (b) t = 800 and (c) t = 850. For $t \leq 700$.

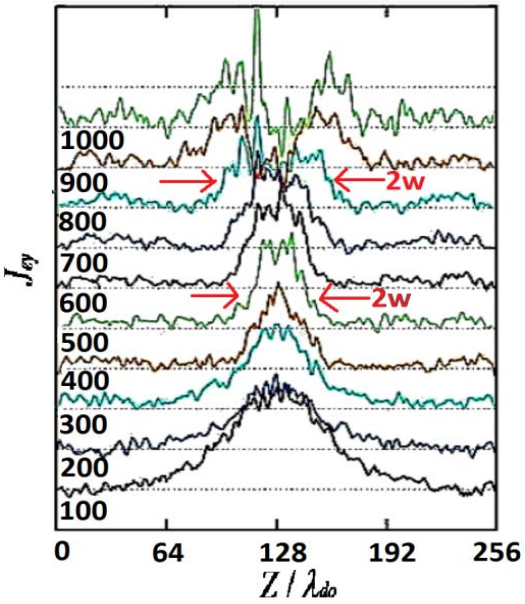

Fig. 1. Current $J_y(z, t)$; the numbers in the panels are normalized time; the ECL thins until t ~ $500\omega_{po}^{-1}$ and then it broadens.

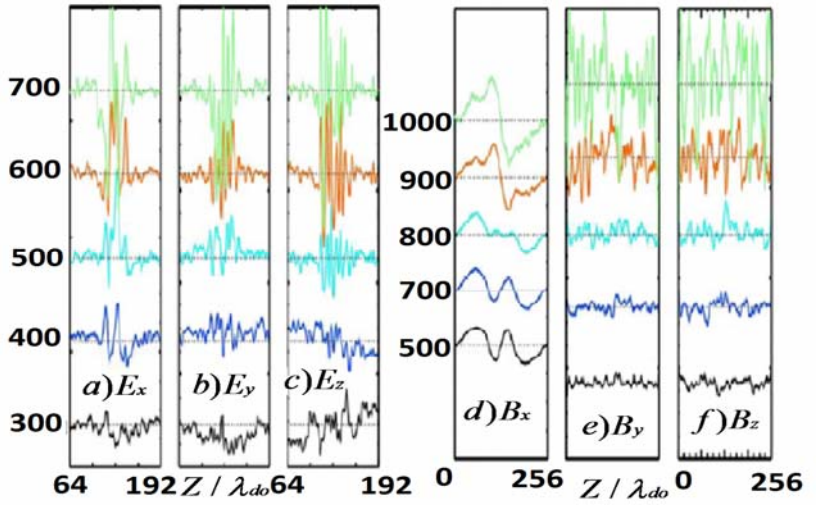

Fig. 2. Temporal evolution of fluctuations in (a) E_x, (b) E_y, (c) E_z and in magnetic fields (d) b_x, (e) b_y and (f) b_z.

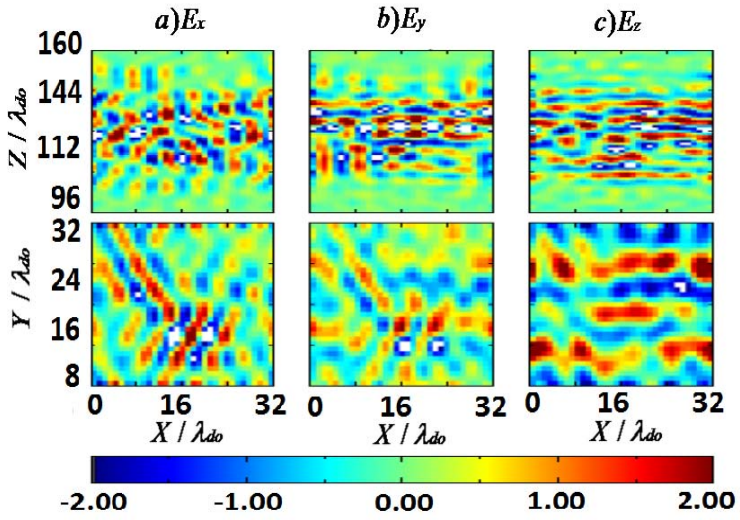

Fig. 3. Wave structure at t = 700: $E_x(x,z)$, $E_y(x,z)$ and $E_z(x,z)$ in top panels from left to right in the x-z plane at y = 16 and bottom panels in the x-y plane at z = 128.

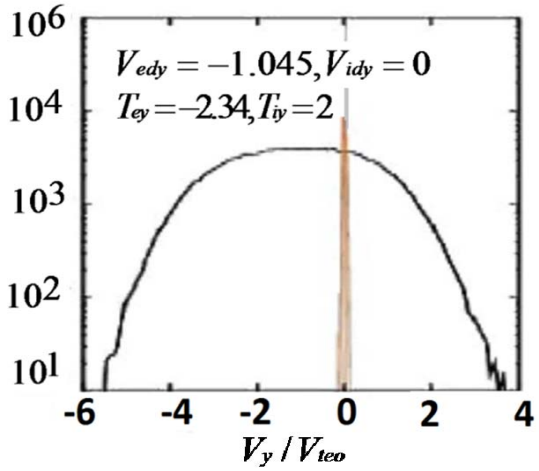

Fig. 4. Electron and ion Velocity distribution functions at t= 500 ω_{peo}^{-1}.

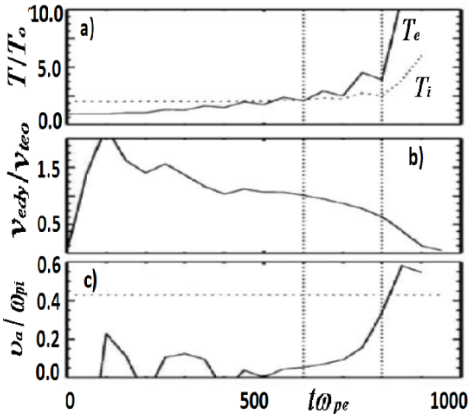

Fig. 5. Temporal evolution: (a) Electron (solid) and ion (dotted) temperatures T_{ey} and T_{iy}, (b) relative drift V_{edy} and (c) anomalous collision frequency ν_a.

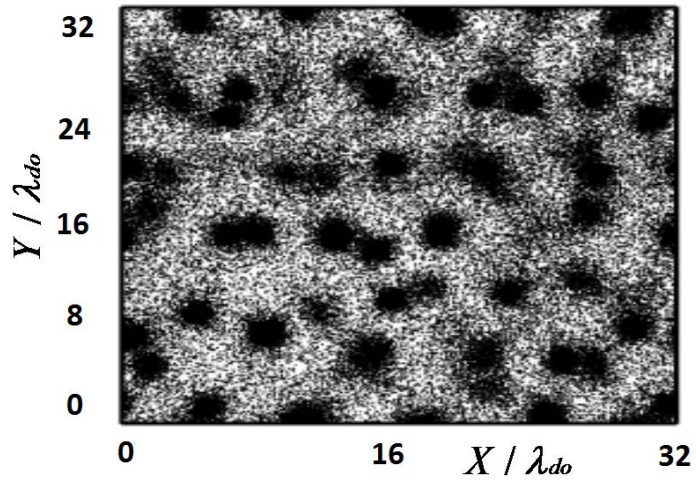

Fig. 6. Spatial distribution of electrons in the x-y plane in the central ECL ($124 < z < 132$); bunched electrons are seen.

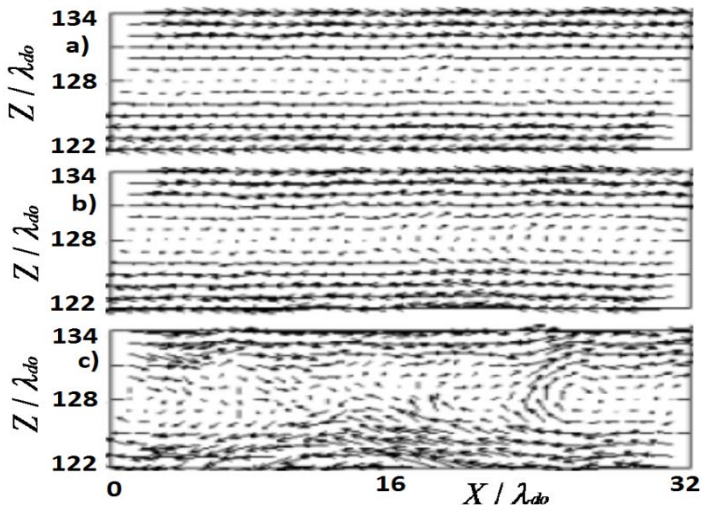

Fig. 7. Vector plot of **B** in the x-z plane at (a) $t = 700\omega_{po}^{-1}$, (b) $t = 800\omega_{po}^{-1}$ and (c) $t = 850\omega_{po}^{-1}$. For $t \leq 700\omega_{po}^{-1}$, **B** remains aligned along x until suddenly t ~700, followed by the generation of b_z.